Observation of intermittency in an experimental turbulent double-helix flux rope

D.A. Schaffner[1], V.S. Lukin[2], A. Wan[1] and M.R. Brown[1]

[1] Swarthmore College, Swarthmore, PA, USA
[2] Naval Research Laboratory, Washington, DC, USA

E-mail: `dschaff2@swarthmore.edu`

Abstract. We have previously generated elongated Taylor double-helix flux rope plasmas in the SSX MHD wind tunnel. These plasmas are remarkable in their rapid relaxation (about one Alfvén time) and their description by simple analytical Taylor force-free theory despite their high plasma β and high internal flow speeds. We discuss here the possibility that the turbulence facilitating access to the final state supports coherent structures and intermittency revealed by non-Gaussian signatures in the statistics. Comparisons to a two-fluid simulation show a similarity in several statistical measures.

1. Overview

Flux ropes observed in the heliosphere have two striking properties. First is their rapid emergence. Whether in the magnetosphere or in the solar corona, these large scale structures emerge rapidly, often in just a few Alfvén crossing times of the system. Second is their long lifetimes. Once formed, these structures persist for long times despite being embedded in turbulent MHD plasma.

Flux ropes have recently been observed *in situ* at the subsolar magnetopause [1]. In this remarkable coordinated observation using three THEMIS spacecraft, a flux rope is caught in the process of forming, revealing properties that are fundamentally 3D. Since magnetospheric flux ropes evolve rapidly, observations of flux ropes in the magnetosphere tend to be detected at later stages of their evolution. The newly formed flux rope reported here appeared to be flanked by two active X-lines as part of the formation process.

Flux ropes are also observed remotely in the solar atmosphere [2]. On July 19, 2012, an eruption occurred on the solar surface producing dynamical magnetic activity resulting in a destabilized flux rope, the acceleration of a fast ($1000\ km/s$) coronal mass ejection, and a long-lived solar flux loop. The long-lived structure is remarkable in its nearly semi-circular topology, and the persistence of a "coronal rain" from the loop top for nearly 24 hours. The observation was made with the Solar Dynamics Observatory's AIA instrument on the sun's lower right hand limb. This represents the first direct evidence of a fast CME driven by the prior formation and destabilization of a coronal magnetic flux rope.

It is interesting to note that in MHD simulations, the peak in the mean square current density $\langle j^2 \rangle$ is also achieved rapidly, within a fraction of an Alfvén time. At this time, the turbulence is fully developed, the peak of small scale activity is achieved, and coherent structures appear.

We have recently reported on the observation of a long-lived helical flux rope called a Taylor double-helix in the SSX MHD wind tunnel [3]. The Taylor double-helix is the natural relaxed state of MHD plasma confined in a long, perfectly conducting cylinder [6]. In the case of an infinite cylinder, the minimum energy state has a helical pitch of $ka = 1.234$, where k is the wave number associated with the z axis.

In the SSX experiments, a magnetized plasma gun launches a magnetized plasma plume into a long flux conserving cylinder. The plasma rapidly relaxes to the double-helix state in about 1 Alfvén crossing time and subsequently decays resistively. In the paper, we postulated that the physics of selective decay was at play as the initially turbulent plasma relaxed to the double-helix state. The selective decay hypothesis posits that the energy selectively decays relative to the magnetic helicity because the energy spectra peaks at higher wave numbers, where dissipation is higher [7]. The wind tunnel's minimum energy state possesses $ka = 1.292$, which is within 5% of the infinite cylinder's $ka = 1.234$.

Servidio et al. [8, 9] detail simulations which observe the rapid and simultaneous

magnetohydrodynamic relaxation into localized patches of plasma with near alignment of **J** and **B**. These patches of locally relaxed plasma can then negotiate with adjacent patches to reach a globally relaxed state on a longer time scale. However, many of the characteristics of the relaxed state will be evident locally. This localized relaxation might explain the rapidity of the transition observed in the double-helix plasmas. A fully relaxed Taylor state would be expected to have a flat lambda profile (where $\nabla \times B = \lambda B$ governs the equilibrium). The reported lack of a flat radial lambda profile could also be a consequence of a patchy relaxation.

We suspect that the MHD turbulent flow in the SSX wind tunnel contains patches of locally relaxed plasma with reconnection sites at the boundaries. A fully relaxed flow might be expected to exhibit Gaussian statistics in its fluctuations and power law behavior for the power spectra. A flow containing coherent structures and reconnection sites should exhibit non-Gaussian statistics. Simulations show that coherent structures appear rapidly, in less than one dynamical time. Large numbers of reconnection sites can be identified statistically in MHD turbulence studies [10, 11]. A statistical way to find these coherent structures is to identify rapid changes in the magnetic field vector. A useful technique is to generate a probability distribution function PDF of vector increments [14, 15].

Greco, *et al* [14] identified intermittent structures in MHD turbulence simulations using statistical techniques then connected the structures with regions of high current density. Using data from a high resolution 3D MHD simulation, they constructed PDFs of magnetic field vector increments $\Delta\mathbf{B} = |\mathbf{B}(s + \Delta s) - \mathbf{B}(s)|$ for two scale separations Δs; one much smaller than the correlation scale and another about $2\ \lambda_C$. They found that the PDF of $\Delta\mathbf{B}$ at the larger increment was close to Gaussian indicating that increments larger than the correlation scale are normally distributed. However, the PDF at the smaller increment had substantial tails in the distribution and furthermore, had the same distribution as the PDF of a component of the current density, indicating that the non-Gaussian statistics were correlated with intense current sheets. They also compared the identification of discontinuities using the spatial interval method described above with coherent structures identified using (PVI) intermittency statistics and found the techniques to be similar.

In a follow-up investigation, Greco, *et al* [15] studied the statistics of ACE solar wind data as well as 2D and 3D simulation data using the same techniques. Time series were analyzed for the solar wind data while spatial separations were analyzed from the simulations. First, they found that the ACE solar wind data had nearly identical increment PDFs to the 2D simulation data. Second, they were able to correlate specific features in the 2D simulation to departures from Gaussian statistics in the PDF. A narrow inner peak is super-Gaussian and corresponds to low values of fluctuations in the lanes between magnetic islands. An intermediate range is sub-Gaussian and corresponds to fluctuations in current cores inside magnetic flux tubes. Finally, at several standard deviations, there are super-Gaussian wings corresponding to coherent small-scale current sheet-like structures that form the sharp boundaries between the magnetic flux tubes.

Non-Gaussian statistics and characteristic coherent structures are initiated almost identically in dissipative and ideal systems [16]. Therefore we postulate that the origins of coherence and intermittency are essentially ideal, with dissipation acting only to limit growth of the smallest scale structures. The fact that our Lundquist number is modest (S = 1000) shouldn't impact the emergence of coherent structures.

We are interested here in the decay phase of the double-helix, in particular, processes that rapidly evolve the state such as patchiness and the evolution of coherent structures. We present MHD turbulence statistics that suggest the emergence of non-Gaussian structures.

2. Experiment

The flux ropes under investigation are formed in a wind-tunnel configuration of the Swarthmore Spheromak Experiment. A copper cylindrical flux conserver serves as the tunnel capped by two plasma gun electrodes whose extent limits the length of the tunnel to 86cm as can be seen in Figure 1. The radius of the cylinder is 7.75cm making the aspect ratio of the this configuration, L/a = 11. Though slightly shorter than the tunnel reported in previous work [3], the aspect ratio is considered still large enough for comparison to an infinite cylinder in Taylor relaxtion theory. The plasma itself is formed by the discharge of a 1mF, 4.0kV capacitor across a few centimeter gap between the tunsten-coated gun inner electrode and outer wall into a puffed volume of hydrogen gas. After ionization, currents of over 80kA across the gap push plasma into the main section of the flux conserver through $v \times B$ forces. Magnetic coils coaxial to the gun electrode and flux conserver contributes the stuffing flux which allows for the formation of a spheromak at the gun edge. Given the high aspect ratio, the spheromak tilts, eventually forming a twisted double-helix Taylor state; this sequence has been shown to occur in a very short time span [3]. For this discharge configuration, the amount of current needed to push spheromaks off of the gun and into the main chamber is maintained for approxmimately $30\mu s$ (~ 20-$50\mu s$ from initial discharge). This suggests that perhaps these shots consists of either elongated spheromak-like structures or a series of spheromaks in a row.

Magnetic fluctuations are measured using an arrayed $\dot{B}$ probe; $\dot{B}$ in three directions (r, θ and z) is measured using 3 orthogonally-oriented 0.3mm single loop coils at 16 locations separated by 0.4cm and beginning 1cm from the cylindrical axis. Signals are aquired using a DTaq digitizer at 14-bit resolution and 65MHz sampling rate. Magnetic field vectors are computed through numerical integration of the $\dot{B}$ signal. Mach number fluctuations, as a proxy for velocity fluctuations are measured using a Mach probe oriented along the axial/z-axis [19] and located 1.5cm from the inner edge of the flux conserver. Density measurements are made using a He-Ne (633nm) laser interferometer at a diameter 21.5cm from the midplane toward the plasma source. In the data presented here, it is assumed that the plasma has already achieved a relaxed Taylor state by the time it reaches the midplane where most of the diagnostics are located. The chamber is

pumped down to $\sim 6 \times 10^{-8}$ Torr and undergoes a helium glow discharge between runs so it is assumed that any influence on the plasma by impurities is low.
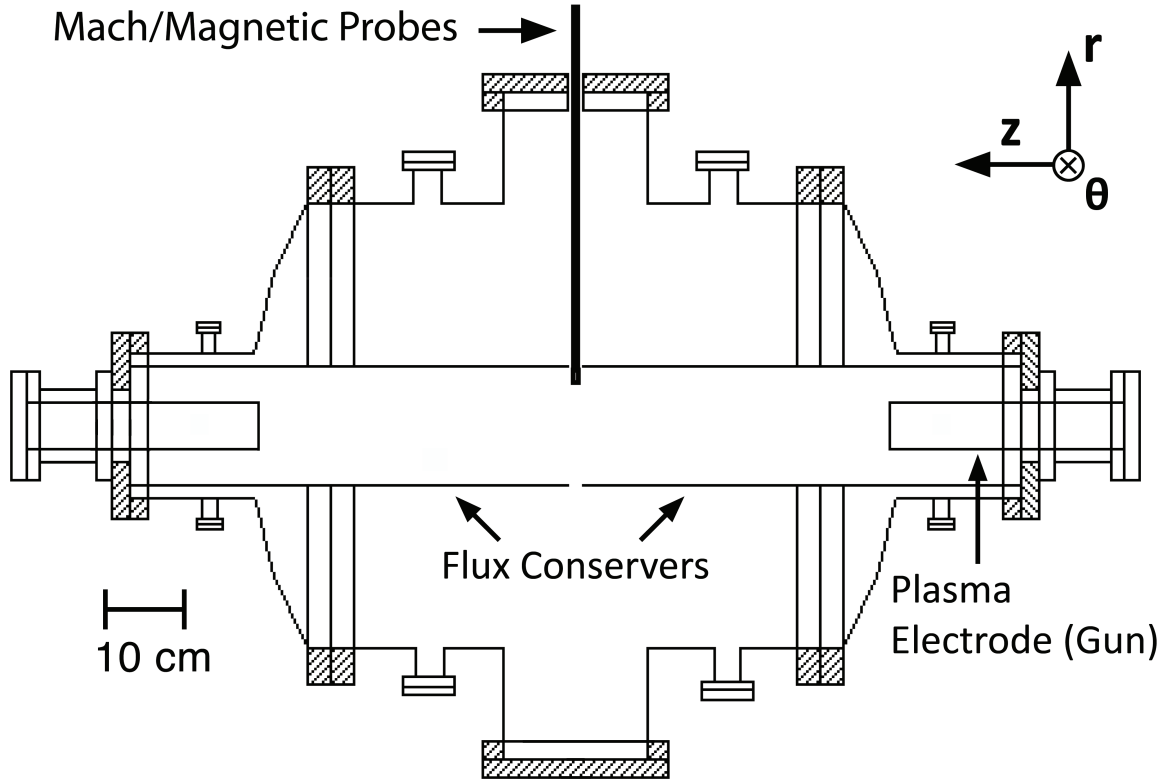

Figure 1. SSX Diagram.

3. Results

The SSX produces flux-rope plasma that persists on the order of $120\mu s$. Figure 2 shows a timeseries of numerically integrated B-field—$|B| = \sqrt{B_r^2 + B_\theta^2 + B_z^2}$—for the innermost tip (1cm from the cylindrical axis), interferometer density, n, Mach probe measured Mach number, M, and discharge current, I_{gun} for a sample single shot and for an average of 75 shots. For time analysis, the shots are divided into epochs to account for the dynamical nature of the plasma discharges as indicated by the dashed lines in Figure 2. The formation/selective-decay epoch spans from 30 to 40 μs. As shown previously in [3], the selective-decay of the plasma into a Taylor state likely occurs in this time range. The equilibrium epoch ranges from 40 to 60 μs and is the period of turbulent fluctuations most closely analyzed here. This time range sees a generally stable period of fully developed turbulence balanced between the sourced plasma from the gun and resistive/viscous effects that degrade the magnetic fields and flows. The epoch from 60 μs on is considered the decay epoch and represents the flux-rope structure's resistive and viscous dissipation. Clearly, as in Figure 2(a), the magnetic field diffuses away by

Table 1. Plasma parameters during the equilibrium epoch for this configuration of SSX.

| Parameter	Value
V_a	$240 km/s$
f_{ci}	$7.6 MHz$
Axial τ_A	0.3μs
Radial τ_A	3.5μs
ρ_i	0.091cm
δ_i	0.51cm
C_s	31km/s
β	0.0967

120μs. Remaining unmagnetizied plasma, however, has been shown to persist for many hundreds of microseconds.

In the equilibrium epoch, the average magnetic field is 5kG and average density is 2×10^{15} cm^{-3}; thus, radial and axial Alfvén transit times are 0.3 and 3.5μ respectively. Ion temperature is measured using an ion Doppler spectrometer system at the midplane. Background ion temperatures (i.e. average temperatures made avoiding large spikes in signal) are on the order of 20eV. Though not measured in this dataset, previous measurements of electron temperature suggest a value of 10eV for this system. Combined with the average field and density values measured, estimates of ion gyrofrequency (f_{ci}), ion gyroradius (ρ_i) and ion inertial length (δ_i) can be made. These values are listed in Table 1. Of particular note, the ratio of system size to ρ_i is large, r/$\rho_i \cong$ 80, suggesting that the influence of the wall on plasma dynamics is minimal.

The density trace in Figure 2(b) shows peaking in the formation epoch, but an eventual drop to approximately 1×10^{15}cm^{-3} for the majority of the discharge. The initial peaking is likely due to the initial spheromak formation, where plasma is being pushed into the tunnel, but before the threshold for break-off is achieved. The Mach number trace is on average positive indicating flow predominately away from the gun source as would be expected. The average Mach number during the equilibrium epoch is M=0.4 which for the sound speed listed in Table 1 yields an average flow speed of 12km/s. It is likely that flow speeds toward the center can be even higher. Indeed, a time of flight estimate based on the axial separation distance between the interferometer measurement and the midplane $\dot{B}$ measurement suggests a bulk plasma flow of 20km/s.

It can also be observed that the decay time for magnetic field and Mach number, during the dissipation epoch, are on the same order. This suggests a Prandl number of order one. That is, neither plasma resistivity nor flow viscosity is dominant for these discharges.

Given the dynamical nature of these plasmas, the spectral decomposition has been approached using a Wavelet technique rather than with purely Fast Fourier Transforms
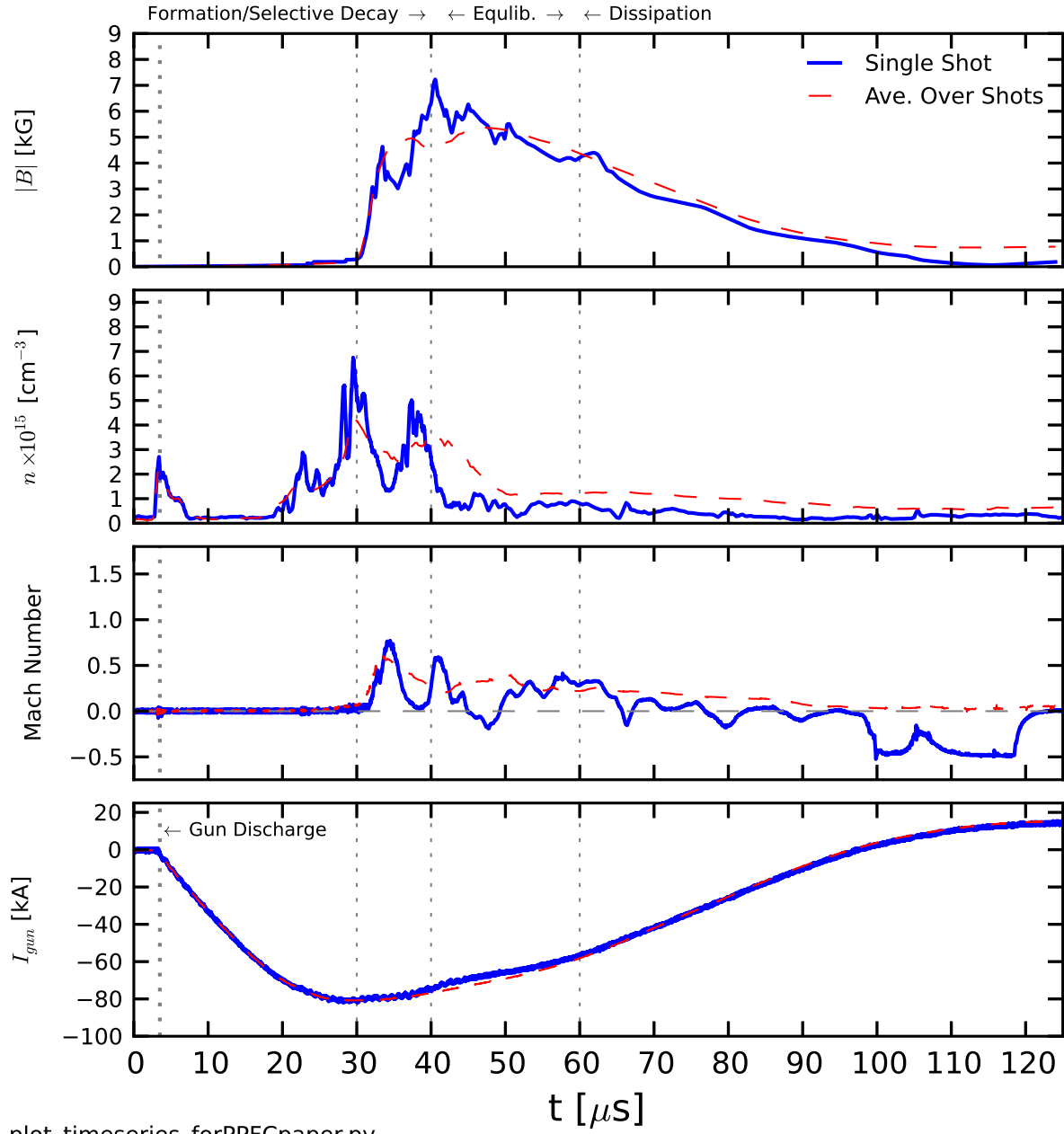
Figure 2. Timeseries of (a) Magnetic Field magnitude, (b) Density, (c) Mach Number, and (d) Discharge current. An example single shot is shown (blue line) as well as the average trace for 75 shots (red dashed).

(FFT). This wavelet technique has been shown to be useful in situations where data may be non-stationary and provides a more accurate method for simulaneous spectral and temporal decomposition then a windowed Fourier transform because it applies a transform and many scales rather than a single scale [20]. To achieve better resolution in frequency space, a six-order Morlet mother wavelet has been used. Morlet wavelet scales (i.e. frequencies) are generally well matched to Fourier scales, though since we are most interested here in power spectral densities (PSD), the choice of wavelet is not critical [20]. A wavelet decomposition for a single shot $\dot{B}$ timeseries is shown in Figure 4 with the wavelet scale converted to a Fourier frequency as the y-axis and time as the x-axis. The color scale corresponds to the normalized fluctation power. Changes in the spectral nature can be seen with time: higher frequency fluctuations grow up and peak around 30μs, hold stable until about 60μs, and then begin to dissipate. This change in flucutuations supports the division of the data into epochs.


plot_wavelet_BMDspec_forPPFCpaper.py
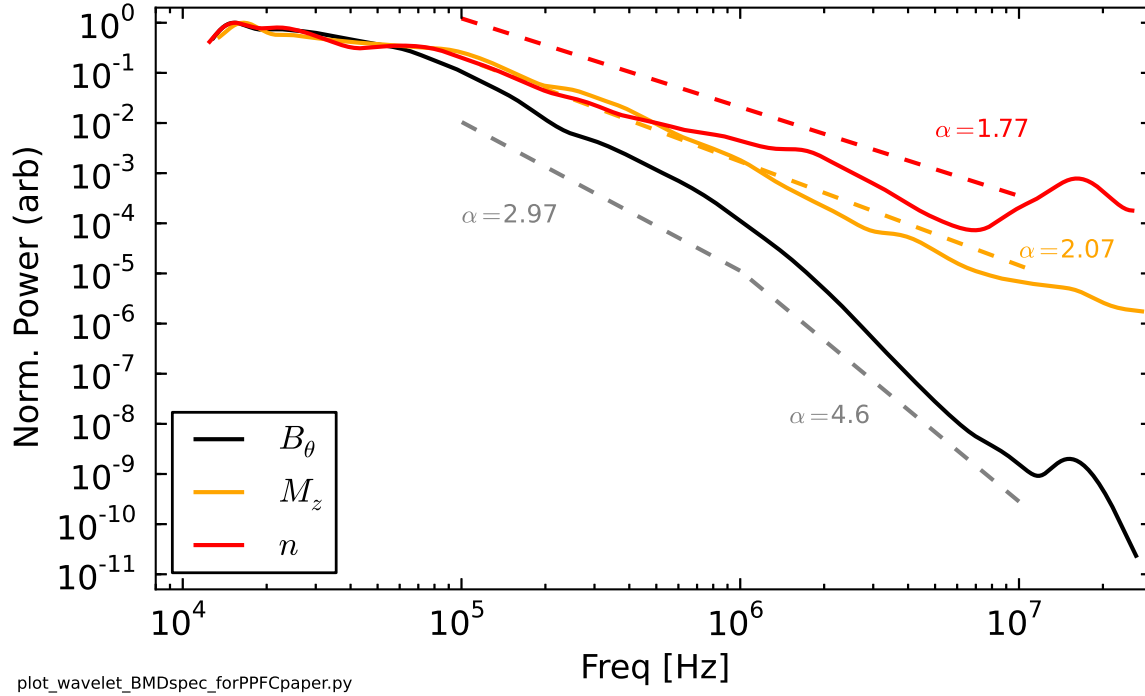
Figure 3. Wavelet Spectrum of B-field, density, and Mach number fluctuations for the equilibrium epoch, 40 to 60μs.

The reduced power spectra for B-field, density and Mach number fluctuations are presented in Figure 3. The B-field curves are produced by first taking a wavelet transform of the $\dot{B}$ timeseries (for any one of the orthogonal components), yielding an array with $\dot{B}$ fluctuation power as a function of both time and frequency as in Figure 4, and scaling the $\dot{B}$ power by f^2 in order to recover actual B-field fluction power. This approach is derived from the assumption that the B-field fluctuations are able to be Fourier decomposited such that

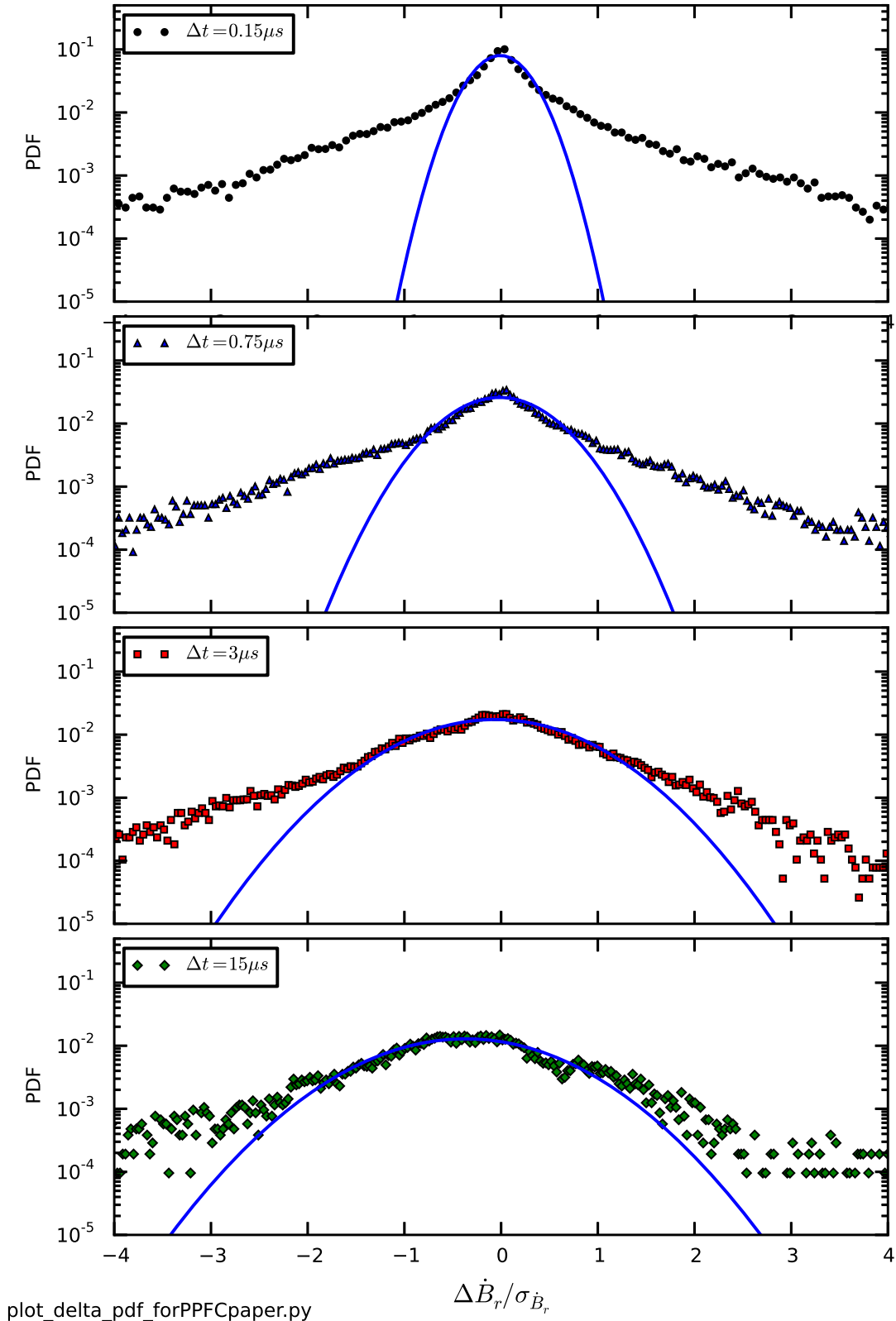$$\frac{d}{dt}B(t) = \frac{d}{dt}B_0 e^{i2\pi f} \sim ifB \tag{1}$$
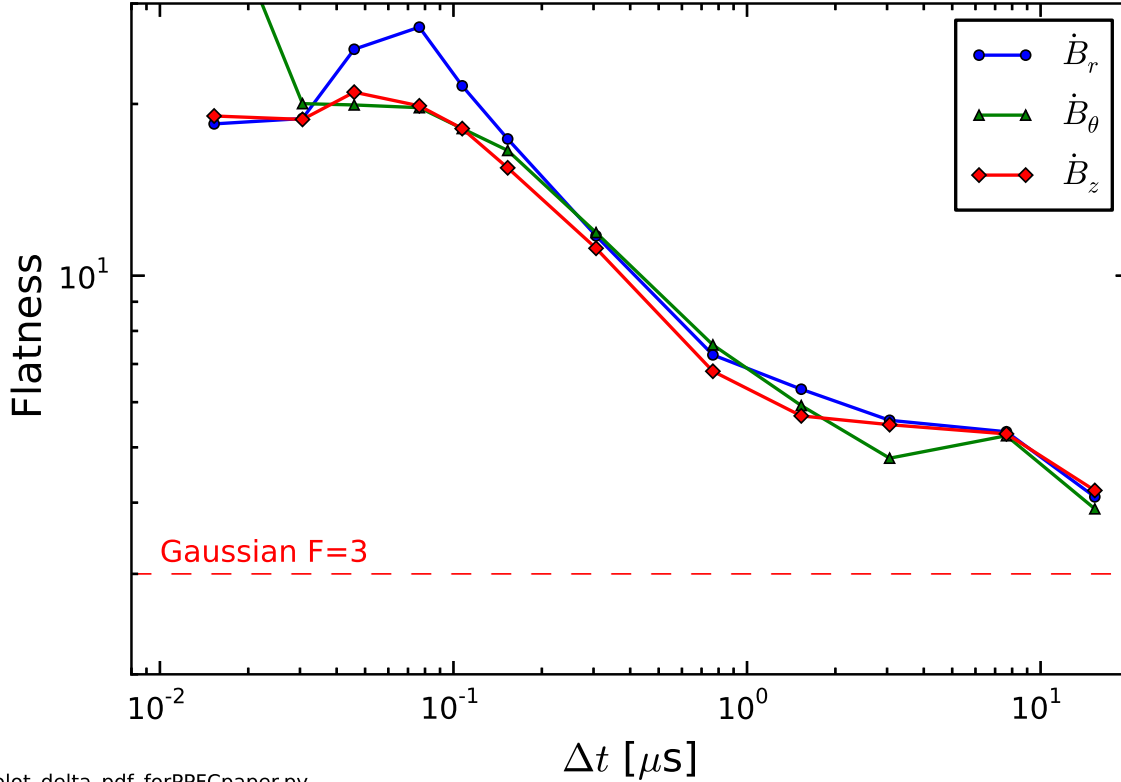
plot_contour_Bwaveletspec_forPPFCpaper.py
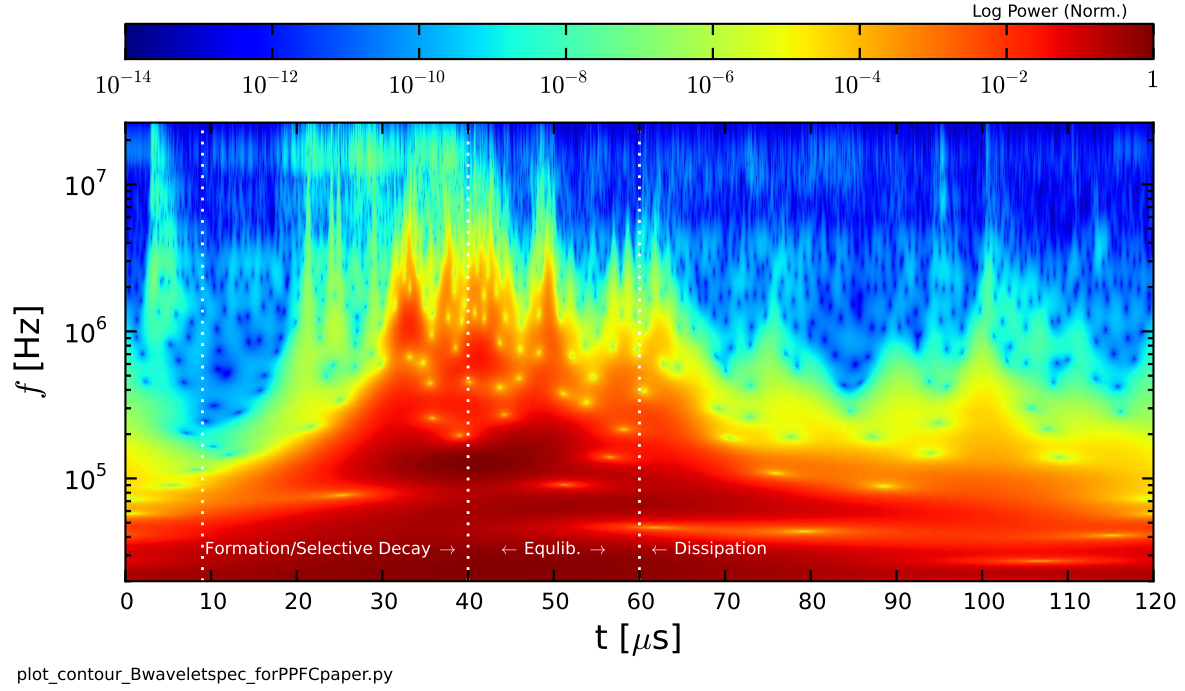
Figure 4. Wavelet Power Spectrum of $\dot{B}_z$ as a function of time for a single shot (same as that shown in Figure 2)

plot_autocorr_forPPFCpaper.py
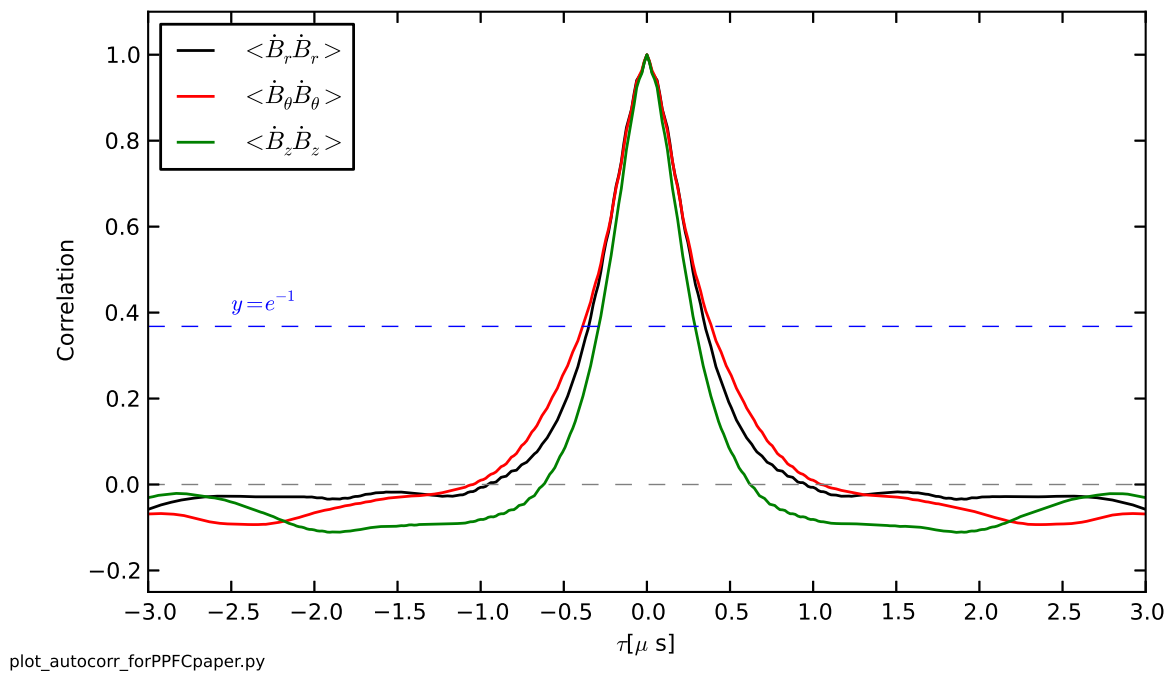
Figure 5. Autocorrelation function for $\dot{B}$ fluctuations in the time range 40 to 60 μs.

plot_delta_pdf_forPPFCpaper.py

Figure 6. PDFs of $\Delta\dot{B}$ in the time range 40 to 60 μs normalized to the standard deviation for each list.

plot_delta_pdf_forPPFCpaper.py

Figure 7. The flatness of the PDFs as a function of Δt. A flatness of 3 would indicate a perfectly Gaussian distribution. A fairly linear slope between 0.1 and $1\mu s$—corresponding to the frequency range of 1MHz to 10MHz—suggest a power-law like relationsihp between the flatness and the timestep.

resulting in the relationship between $\tilde{B}(f)$ and $\tilde{\dot{B}}(f)$ as

$$|\tilde{B}(f)|^2 = \frac{1}{f^2}|\tilde{\dot{B}}(f)|^2 \tag{2}$$

where $|\tilde{x}(f)|^2$ is the PSD. The same relationship applies for the Wavelet Transform. Once converted into a B-field power array, the 1-D spectrum is calculated by summing over a certain time region—in this case the equilibrium epoch of 40 to $60\mu s$. A similar approach is made for density and Mach number, though without the frequency scaling.

All three curves have roughly linear behavior in the spectral region between 50kHz and 10MHz. A power-law fit of spectral power to frequency ($P(f) \sim f-\alpha$) is made for density and Mach number in this frequency range using a maximum likelihood estimation method [22] (MLE) yielding exponents of $\alpha = 1.57$ for the density spectrum and $\alpha = 1.62$ for the mach spectrum which is a proxy for the velocity spectrum in this experiment. An exponent of 1.62 for velocity is very close to the typical Kolmogorov exponent of -5/3 = 1.66 for hydrodynamic flow fluctuations.

The magnetic field spectrum appears to have two separate regions: a shallower sloped region between 50kHz and 1MHz and a steeper sloped region between 1MHz and 10MHz. MLE fits for these regions give exponents of $\alpha = 2.47$ (shallower) and

$\alpha = 4.36$ (steeper). Both the plots and the fits indicate that the spectra slope for B-field fluctuations is steeper than that for Mach/velocity fluctuations. This is perhaps indicative of a dissipation mechanism that is reached at lower frequencies for B-field than for velocity. Dissipation may also be an explanation for the perceived break in slope at around 1MHz which from a canonical turbulent spectrum point of view may be a transition from the inertial range to the dissipation range. One possible dissipation mechanism is coupling to the ion gyrofrequency which for the equilibrium epoch is 7.6MHz which is toward the low end of the steeper spectrum. Another explanation is a breakdown of the Taylor hypothesis (frozen-in flow). The average axial flow as indicated by the Mach probe is 12km/s. Given the width of the Mach probe ($\sim 1.3cm$), the Taylor hypothesis would be valid only for frequencies above 1MHz. Thus the break in slope could be representative of a transition between fluctuations due to both spatial and temporal changes (< 1MHz) and those due to only temporal changes (> 1MHz).

An alternative reason could lie in the decorrelation of fluctuations. Figure 5 shows the autocorrelation function for $\dot{B}$ for each of the three axes again during the equilibrium epoch. A decorrelation time can be defined as the τ at which the autocorrelation function crosses zero. For $\dot{B}_r$ and $\dot{B}_\theta$, this occurs at about $\tau = 1\mu$s which corresponds to a fluctuation scale of 1MHz.

While spectra can be useful for obtaining the relative rate of energy transfer amongst injection, inertial and dissipation scales, they can obscure other signatures of turbulence that can only be seen when looking at higher integral moments. One technique for investigating these higher moments is to construct probability distribution functions (PDF's) from the data at different timescales and then directly calculate moments. The variation in the moments of PDFs as a function of timescale has been shown to be linear for fully-developed fluid turbulence [23]. One can introduce a timescale into the timeseries by filtering [23, 24] or by taking differences of the data points at different time steps [14, 15]. This latter technique is used here where a series of $\Delta \dot{B}$ increments is constructed for a variety of timesteps, τ, as in

$$\Delta \dot{B}_\tau(t) = \dot{B}(t + \tau) - \dot{B}(t) \tag{3}$$

A series of these PDFs for the equilibrium epoch timeseries is shown in Figure 6 for τs of 0.15μ, 0.75μs, 3μs and 15μs which corresponds to filtering the timeseries above frequencies of 6.6MHz, 1.3MHz, 333kHz, and 66kHz respectively. The PDFs are normalized to the root mean square value of the increments and to the total area. A Gaussian function is fit to each distribution. One can clearly see a transition from non-Gaussian distributions for small τs to more Gaussian distribution for larger τs. The features of the non-Gaussian distributions are indicative of intermittency in the signal; the fat tails signify large swings in the values of the timeseries and the timestep indicates the relative temporal size of the intermittent events.

The level of intermittancy as a function of τ can be quantified using a calculation of the flatness defined as [21]

$$F(\tau) = \frac{S_4(\tau)}{S_2(\tau)^2} \tag{4}$$

where $S_p(\tau)$ is the p-th order moment or sturcture function for the distribution of increments, $\Delta\dot{B}$, as in

$$S_p(\tau) = \int_{-x_{max}}^{x_{max}} P(\Delta\dot{B})(\Delta\dot{B})^p dx \tag{5}$$

with x representing a histogram bin width. An exact Gaussian distribution would have a flatness equal to 3.

The resulting function for flatness is shown in Figure 7 for each of the three $\dot{B}$ measurements. The plot shows the trend toward Gaussian (as represented by the dashed line at F=3) as the timestep is increased. An increase in flatness signifies an increase in the intermittency observed in the PDF—a large jump occurs at a $\tau = 1\mu$ corresponding to a frequency of 1MHz. Recent work in this vein on solar wind measurements has speculated that such a change might be expected at the transition from inertial to dissipation range turbulence [24]. The large change in flatness observed supports the wavelet spectrum evidence for onset of dissipation beyond 1MHz.

4. Discussion

The observation of non-Gaussian values for flatness in the PDFs, and the trend for increasing flatness with decrease in timestep is a strong indication for the presence of intermittent fluctuations and/or coherent structures in the plasma which could not be observed with spectra alone. The physical origin of these coherent structures in the SSX plasma has not yet been identified. As seen in previous simulation work (i.e. [13], the coherent structures can be matched to the presence of current sheets which in turn could be the site of a reconnection layer. Given the observation of reconnection in past SSX work [5, 4], there is a strong likelihood that such events are present in the current SSX configuration though perhaps at a smaller scale.

References

[1] Oieroset, M., T. D. Phan, J. P. Eastwood, M. Fujimoto, W. Daughton, M. Shay, V. Angelopoulos, F. S. Mozer, J. P. McFadden, D. E. Larson, and K. -H. Glassmeier, Direct evidence for a three-dimensional magnetic flux rope flanked by two active magnetic reconnection X-lines at the Earth's magnetopause, Physical Review Letters, Vol. 107, 165007, 2011

[2] S. Patsourakos, A. Vourlidas, and G. Stenborg. Direct Evidence for a Fast Coronal Mass Ejection Driven by the Prior Formation and Subsequent Destabilization of a Magnetic Flux Rope, ApJ 764 125, 2013

[3] T. Gray, M. R. Brown, and D. Dandurand, Observation of a Relaxed Plasma State in a Quasi-Infinite Cylinder, Phys. Rev. Letters 110, 085002 (2013).

[4] Three-dimensional reconnection and relaxation of merging spheromak plasmas T. Gray, M. R. Brown, C. D. Cothran, and V. S. Lukin Physics of Plasmas 17, 102106 (2010)

[5] C. D. Cothran, M. R. Brown, T. Gray, M. J. Schaffer, and G. Marklin, Phys. Rev. Lett. 103, 215002 (2009).

[6] J. B. Taylor, Rev. Mod. Phys. 58, 741 (1986).

[7] W.H. Matthaeus and D. Montgomery, Ann. N.Y. Acad. Sci. 357, 203 (1980).

[8] Servidio, S., Matthaeus, W. H., and Dmitruk, P.: Depression of Nonlinearity in Decaying Isotropic MHD Turbulence, Phys. Rev. Lett., 100, 095005, doi:10.1103 Phys. Rev. Lett.100.095005, 2008.

[9] Servidio, S., Dmitruk, P., Greco, A., Wan, M., Donato, S., Cassak, P. A., Shay, M. A., Carbone, V., Matthaeus, W. H., Magnetic reconnection as an element of turbulence, Nonlinear Processes in Geophysics, Vol. 18, p. 675-695, 2011.

[10] Servidio, S., Matthaeus, W. H., Shay, M. A., Cassak, P. A., and Dmitruk, P.: Magnetic Reconnection in Two-Dimensional Magnetohydrodynamic Turbulence, Phys. Rev. Lett., 102, 115003, doi:10.1103/PhysRevLett.102.115003, 2009.

[11] Servidio, S., Matthaeus, W. H., Shay, M. A., Dmitruk, P., Cassak, P. A., and Wan, M.: Statistics of magnetic reconnection in two- dimensional magnetohydrodynamic turbulence, Phys. Plasmas, 17, 032315, doi:10.1063/1.3368798, 2010a.

[12] Servidio, S., Wan, M., Matthaeus, W. H., and Carbone, V.: Local relaxation and maximum entropy in two-dimensional turbulence: Phys. Fluids, 22, 125107, doi:10.1063/1.3526760, 2010b.

[13] Servidio, S., Greco, A., Matthaeus, W. H., Osman, K. T., and Dmitruk, P.: Statistical association of discontinuities and reconnection in magnetohydrodynamic turbulence, J. Geophys. Res., 116, A09102, 111, doi:10.1029/2011JA016569, 2011.

[14] Greco, A., Chuychai, P., Matthaeus, W. H., Servidio, S., and Dmitruk, P.: Intermittent MHD structures and classical discontinuities, Geophys. Res. Lett., 35, L19111, doi:10.1029/2008GL035454, 2008.

[15] Greco, A., Matthaeus, W. H., Servidio, S., Chuychai, P., and Dmitruk, P.: Statistical Analysis of Discontinuities in Solar Wind ACE Data and Comparison with Intermittent MHD Turbulence, Astrophys. J., 691, L111, doi:10.1088/0004-637X/691/2/L111, 2009.

[16] Wan, M., Oughton, S., Servidio, S., and Matthaeus, W. H.: Generation of non-Gaussian statistics and coherent structures in ideal magnetohydrodynamics, Phys. Plasmas, 16, 080703, doi:10.1063/1.3206949, 2009.

[17] Wan, M., W. H. Matthaeus, H. Karimabadi, V. Roytershteyn, M. Shay, P. Wu, W. Daughton, B. Loring, and S. C. Chapman, Intermittent Dissipation at Kinetic Scales in Collisionless Plasma Turbulence, Physical Review Letters, Vol. 109, 195001, 2012.

[18] Osman, K. T., Matthaeus, W. H., Greco, A., and Servidio, S.: Evidence for Inhomogeneous Heating in the Solar Wind, Astrophys. J., 727, L11, doi:10.1088/2041-8205/727/1/L11, 2011.

[19] X. Zhang, D. Dandurand, T. Gray, M. R. Brown, and V. S. Lukin, "Calibrated Cylindrical Mach Probe in a Plasma Wind Tunnel", Review of Scientific Instruments 82, 033510 (2011).

[20] C. Torrence, G.P. Compo, A practical guide to wavelet analysis. Bull. Am. Meteorol. Soc. 79, 6178 (1998). doi:10.1175/1520-0477(1998)079¡0061:APGTWA¿2.0.CO;2

[21] T. Dudok de Wit, O. Alexandrova, I. Furno, L. Sorriso-Valvo, G. Zimbardo, Methods for Characterising Microphysical Processes in Plasmas. Space Sci. Rev. 0038-6308 (2013). 10.1007/s11214-013-9974-9

[22] A. Clauset, C. Rohilla Shalizi, M.E.J. Newman, Power-law distributions in empirical data. SIAM Rev. 51, 661703 (2009). doi:10.1137/070710111

[23] Frisch, U. 1995, Turbulence (Cambridge: Cambridge Univ. Press)

[24] INVESTIGATION OF INTERMITTENCY IN MAGNETOHYDRODYNAMICS AND SOLAR WIND TURBULENCE: SCALE-DEPENDENT KURTOSIS Minping Wan et al., The Astrophysical Journal 744, 171 (2012)